Nonlinear two and three dimensional free surface flows due to moving disturbances

Emilian Părău[1,2], Jean-Marc Vanden-Broeck[3]

April 29, 2006

[1]School of Mathematics and Statistics, University of Birmingham, Edgbaston, Birmingham, B15 2TT, UK
[2]Faculty of Mathematics, West University of Timişoara, Timişoara, Romania
[3]School of Mathematics, University of East Anglia, Norwich, NR4 7TJ, UK

Abstract

Boundary integral equation methods for computing two and three dimensional nonlinear free surface flows are presented. In two dimensions, integral formulations can be derived by using complex variables or Green's functions. Both formulations are shown to yield the same level of accuracy. The formulation based on Green's functions is extended to three dimensions by following Forbes [1] and accurate numerical results are presented for moving distributions of pressure and moving submerged disturbances.

1 Introduction

Over the last 150 years, important progress has been achieved in the calculation of two dimensional free surface waves. This success is largely based on the fact that two dimensional potential flows can be formulated in terms of complex variables and analytic functions. Therefore conformal mappings can be used to map the flow domain (with a free surface) into another convenient domain (without a free surface). Furthermore, Cauchy integral formula can then be used to reformulate the problem as a system of singular nonlinear integro-differential for the unknown shape of the free surface. This equation cannot usually be solved analytically. It is also often difficult to solve this equation numerically, too, but this formulation at least has the advantage that it involves a one-dimensional system (in contrast with the original problem which is two dimensional). This means that very accurate solutions can be obtained with relatively few mesh points.

Boundary integral equation methods for two dimensions can also be derived by using Green's functions. This approach has the advantage that it can be extended for three dimensions.

In this paper we first consider the two dimensional problem of moving pressure and solve it by using boundary integral equations methods based on complex variables and

on Green's functions. We then consider the extension of the Green's function approach to three dimensional problems and present numerical results. The three dimensional scheme is similar to Forbes [1], except that we do not use splines. Other methods for three-dimensional steady problems can be found in Scullen and Tuck [2], Tuck et al. [3]. There are also papers which study the three-dimensional unsteady free-surface flows, as in Cao et al. [4], Scorpio et al. [5] which use a desingularized method, Grilli et al. [6], Xue et al. [7] where higher-order three-dimensional boundary element methods are used. These algorithms are based on a mixed Euler-Lagrange approach to solve the time dependent boundary integral equation formulation. The method was originally developed for two-dimensional unsteady waves by Longuet-Higgins & Cokelet [8]. Other method to study the steady and unsteady potential flows can be found in Nakos and Sclavaunos [9] which use a Rankine Panel method. A recent extensive review of the computations of nonlinear free-surface flows is given by Tsai & Yue [10].

The two dimensional problem for a moving distribution of pressure is considered in Section 2, the two dimensional problem of a piercing object is then considered in Section 3. The numerical results for the three dimensional problems are presented in Section 4.

2 Two dimensional pressure distribution

2.1 Formulation

We consider the two dimensional free surface flow generated by a distribution of pressure moving at a constant velocity U at the surface of a fluid of infinite depth. The fluid is assumed to be inviscid and incompressible and the flow to be irrotational. We choose a cartesian frame of reference moving with the distribution of pressure and assume that the flow is steady. We introduce the potential function $\Phi(x, y)$ so that the velocity is given by (Φ_x, Φ_y). In the flow domain, Φ satisfies

$$\nabla^2 \Phi = 0, \qquad x \in \mathbf{R}, y < \eta(x), \tag{1}$$

with the condition

$$(\Phi_x, \Phi_y) \to (U, 0), \quad y \to -\infty. \tag{2}$$

We denote by $y = \eta(x)$ the equation of the free surface. The kinematic and dynamic boundary conditions give

$$\Phi_x \eta_x = \Phi_y, \quad y = \eta(x), \tag{3}$$

and

$$\frac{1}{2}(\Phi_x^2 + \Phi_y^2) + g\eta + \frac{p}{\rho} = \frac{U^2}{2}, \quad y = \eta(x). \tag{4}$$

Here g is the acceleration of gravity, ρ is the fluid density and p the prescribed distribution of pressure. The choice of the Bernoulli constant on the right hand side of (4) fixes the origin of y. The upstream radiation condition gives

$$(\Phi_x, \Phi_y) \to (U, 0), \quad \eta \to 0, \qquad \text{as } x \to -\infty. \tag{5}$$

The physical quantities are made dimensionless by using U as the unit velocity and the length L of the support of the distribution of pressure as the unit length. The Froude number is defined by

$$F = \frac{U}{\sqrt{gL}}. \tag{6}$$

We now describe the two integro–differential equation reformulations mentioned in the introduction.

The first reformulation relies on complex variables and uses Cauchy integral formula (see for example Asavanant & Vanden-Broeck [11] and Vanden-Broeck & Dias [12]). We introduce in addition to the potential function Φ, the streamfunction Ψ. We choose $\Psi = 0$ on the free surface. We seek the complex function $x' + iy'$ as an analytic function of $\Phi + i\Psi$ in the lower half plane $\Psi < 0$. Here primes denote derivatives with respect to Φ. The method used here is an inverse type method, in which the spatial variables are obtained in terms of the velocity potential and the streamfunction. Applying Cauchy integral formula to $x' + iy' - 1$ on a contour consisting of the free surface and a half circle of arbitrary large radius in $\Psi < 0$ we obtain

$$x' + iy' - 1 = -\frac{1}{2i\pi}\int_{-\infty}^{\infty} \frac{(x'(\xi) - 1 + iy'(\xi))}{\xi - (\Phi + i\Psi)})_{|\Psi=0} d\xi \tag{7}$$

Since $x' + iy' - 1$ tends to 0 as $\psi \to -\infty$, there is no contribution from the half circle. Taking the limit $\psi \to 0$ in (7) and then the real part we obtain

$$x' - 1 = -\frac{1}{\pi}\int_{-\infty}^{\infty} \frac{y_\xi}{\xi - \Phi} d\xi \tag{8}$$

Next we rewrite (4) as

$$\frac{1}{2}\frac{1}{x'^2 + y'^2} + \frac{y}{F^2} + \varepsilon P = 0 \tag{9}$$

where εP is the (prescribed) dimensionless pressure. The integral in (8) is a Cauchy principal value. Substituting (8) into (9) yields a nonlinear integro differential equation for y'. This equation is solved numerically in the next Section.

The second reformulation does not rely on complex variables and involves Green's second identity

$$\int_V (\alpha\Delta\beta - \beta\Delta\alpha) dV = \int_C (\alpha\frac{\partial\beta}{\partial n} - \beta\frac{\partial\alpha}{\partial n}) ds \tag{10}$$

Here C is a closed curve bounding a region V of the plane. The curve C is characterised by its arclength s and its outward normal $\mathbf{n}$. Assuming that α satisfies Laplace equation and that β is the two dimensional free space Green function $g = \frac{1}{4\pi}\ln[(x-x^*)^2 + (y-y^*)^2]$, (10) gives

$$\alpha(x^*, y^*) = r\int_C (\alpha\frac{\partial g}{\partial n} - g\frac{\partial\alpha}{\partial n}) ds \tag{11}$$

Here $r = 1$ when (x^*, y^*) is inside C and $r = 1/2$ when (x^*, y^*) is on C. We now choose $\alpha = \Phi - x$ and assume that C consists of the free surface and a half circle of arbitrary

large radius in the region $y < \eta(x)$. Using the arclength s and describing the free surface parametrically by $x = X(s)$ and $y = Y(s)$ we obtain

$$\frac{1}{2}\mathcal{F}(s^*) = \int_{-\infty}^{\infty} \left[\mathcal{F}(s)\frac{\partial G}{\partial n}(s, s^*) - G(s, s^*)\frac{\partial \mathcal{F}(s)}{\partial n}\right] ds. \tag{12}$$

Here $\phi(s) = \Phi(X(s), Y(s))$, $\mathcal{F}(s) = \phi(s) - X(s)$, $G(s, s^*) = \frac{1}{4\pi}\ln[(X(s) - X(s^*))^2 + (Y(s) - Y(s^*))^2]$ and $\mathbf{n} = (-Y'(s), X'(s))$. The definition of the arclength requires that

$$X'^2 + Y'^2 = 1, \tag{13}$$

Many authors have used the above parametrization in the recent years (see for example Forbes [13], Vanden-Broeck [14]).

The kinematic and dynamic boundary conditions on the free surface are rewritten as

$$\frac{\partial \phi}{\partial n} = 0, \tag{14}$$

and

$$\frac{1}{2}\phi_s^2 + \frac{Y}{F^2} + \varepsilon P = \frac{1}{2}, \tag{15}$$

where ϵP is the dimensionless pressure. In this paper we choose

$$P(s) = \begin{cases} e^{\frac{1}{s^2-1}}, & \text{for } |s| < 1 \\ 0, & \text{otherwise.} \end{cases} \tag{16}$$

The unknown functions $\phi(s)$, $X(s)$ and $Y(s)$ are obtained by solving the nonlinear equations (12)-(15), subject to the radiation condition.

2.2 Numerical scheme

The integro differential equations (8) and (9) were solved numerically by following the procedure outlined in Asavanant & Vanden-Broeck [11]. The reader is referred to that paper for details.

We shall describe the numerical procedure used to solve (12)-(15). We define N equally-spaced points $s_1 = -e(N-1)/2$, $s_i = s_1 + e(i-1)$, $i = 2, ..., N$, where e is the interval of discretization. We chose N to be odd. Here s_1 approximates $-\infty$ and $s_N = -s_1$ approximates $+\infty$. We use the notation $x_i = X(s_i)$, $y_i = Y(s_i)$, etc. The domain of integration for (12) is (s_1, s_N).

In order to satisfy the Bernoulli equation at the first point, we impose

$$y_1 = 0, x_1' = \phi_1' = 1, x_1 = \phi_1 = s_1. \tag{17}$$

Equations (13)-(15) and the trapezoidal rule yields

$$\begin{aligned} x_k' &= \sqrt{1 - y_k'^2} \\ x_k &= x_{k-1} + \tfrac{1}{2}e(x_k' + x_{k-1}') \\ y_k &= y_{k-1} + \tfrac{1}{2}e(y_k' + y_{k-1}') \\ \phi_k' &= \sqrt{1 - 2\tfrac{y_k}{F^2} - 2p_k} \\ \phi_k &= \phi_{k-1} + \tfrac{1}{2}e(\phi_k' + \phi_{k-1}') \end{aligned} \tag{18}$$

for $k = 2, ..., N$.

The values of the functions at the midpoints are calculated by interpolation with two or four points ($x_{k-1/2} = \frac{1}{2}(x_{k-1} + x_k)$ etc.). The equation (12) is evaluated at midpoints $s_{i-1/2}$, $i = 2, ..., N-1$. The integral is approximated by the trapezoidal rule with a summation over the mesh points s_i, $i = 2, \ldots, N$. Substituting (18) yields $N-2$ nonlinear algebraic equations. The last two equations are obtained by imposing the radiation condition by the relations

$$y_1' = 0 \text{ and } -3y_1' + 4y_2' - y_3' = 0. \tag{19}$$

The second of these relations imposes approximately $y_1'' = 0$. This system of N nonlinear equations for the N unknowns $y_1', \ldots, y_N'$ is solved by Newton's method. A similar numerical scheme, but used for another problem which involves Cauchy integral formula can be found in Forbes [13].

The initial guess for the unknowns y_i' is zero when $\varepsilon \ll 1$ or previous computed solutions obtained for slightly different values of F and ε when ε is large.

2.3 Results

The numerical accuracy of the scheme described in the previous section for solving (12)–(15) was checked by varying N and e (see Figure 1). We found that the solutions presented here are independent of N and e within graphical accuracy for $N \geq 200$ and $e \leq 0.1$. In the numerical calculations, the integral from $-\infty$ to ∞ in (12) is replaced by an integral from s_1 to s_N. We found that these upstream and downstream truncations only affects the first and last half wavelength of the free surface profiles. A similar numerical behavior was found in Asavanant & Vanden-Broeck [11].

We compared our numerical solutions with those obtained by using the method of Asavanant & Vanden-Broeck [11] (i.e. by solving (8) and (9))). A typical comparison is shown in Figure 1. Similar results were found for other values of ε and F. The conclusion of the comparison is that numerical results as accurate as those of Asavanant & Vanden-Broeck [11] can be obtained without using complex variables. This suggests that accurate results for three dimensional free surface flows can be obtained by generalising the Green formulation of Section 2 to three dimensions. This is done in Section 4.

3 Two dimensional surface piercing object

Once a solution of (12)–(15) or of (8), (9) has been computed for a given pressure distribution (16), we can replace the free surface under the support $-1 < s < 1$ of the pressure distribution by a rigid surface. Therefore the schemes described in the previous sections provide an inverse method to calculate free surface flows past surface piercing objects or two dimensional "ships". The shape of the ship is given at the end of the calculations by the shape of the streamline under the support of the pressure distribution. One drawback of this approach is that the shape of the ship depends on F. It is therefore desirable to have approaches which enable a direct calculation of the free surface flow past a given surface piercing object. This was achieved by Asavanant & Vanden-Broeck

[11] using complex variables. In this section we explore the corresponding approach using the Green function formulation.

3.1 Formulation and numerical procedure

We shall present results for a parabolic object defined by the equation

$$y = \frac{\varepsilon}{2}(x^2 - 1). \tag{20}$$

In general we might expect a spray or splash at the front of the object (see for example Dias & Vanden-Broeck [15]). Here, we restrict our attention to flows which separate smoothly from the object. The calculation of flows past bodies in finite of infinite depth has received much interest in recent years. Madurasinghe & Tuck [19], Tuck & Vanden-Broeck [20], Farrow & Tuck [17] have computed flows past bodies of arbitrary shape which have either a smooth separation from the body, or a stagnation point on the body in water of infinite depth. Hocking [16] has computed bow flows with smooth separation in water of finite depth. McCue & Forbes [18] have presented computations of bow and stern flows with constant vorticity in finite depth. All these papers computed flows past a two-dimensional semi-infinite body having only one point of separation, whereas in our paper we study flows past finite bodies which have two points of separation: one in front and one at the end of the body.

Let's denote by s_a and s_b the values of s at the left and right separation points. Since we need to find s_a and s_b as part of the solution, we introduce the new variable t by

$$s = s_a + (s_b - s_a)t. \tag{21}$$

The relation (21) maps the unknown interval (s_a, s_b) into the fixed interval $(0, 1)$. The new unknown functions are $\tilde{\phi}(t) := \phi(s)$, $\tilde{X}(t) = X(s)$, $\tilde{Y}(t) = Y(s)$, where s is defined by (21).

The system of nonlinear equations to be solved is now obtained by substituting (21) into (12), (13), (15). This yields the integrodifferential equation

$$2\pi(\tilde{\phi}(t^*) - \tilde{X}(t^*)) = \int_{-\infty}^{\infty} \left[2(\tilde{\phi}(t) - \tilde{X}(t)) \frac{(\tilde{X}(t) - \tilde{X}(t^*))(-\tilde{Y}'(t)) + (\tilde{Y}(t) - \tilde{Y}(t^*))\tilde{X}'(t)}{(\tilde{X}(t) - \tilde{X}(t^*))^2 + (\tilde{Y}(t) - \tilde{Y}(t^*))^2} \right.$$

$$\left. - \ln[(\tilde{X}(t) - \tilde{X}(t^*))^2 + (\tilde{Y}(t) - \tilde{Y}(t^*))^2]\tilde{Y}'(t) \right] dt, \qquad -\infty < t^* < \infty \tag{22}$$

the Bernoulli equation,

$$\frac{1}{2}\left(\frac{\tilde{\phi}_t}{s_b - s_a}\right)^2 + \frac{\tilde{Y}}{F^2} = \frac{1}{2}, \text{ for } t < 0 \text{ or } t > 1 \tag{23}$$

and the arclength equation

$$\tilde{X}'^2 + \tilde{Y}'^2 = (s_b - s_a)^2. \tag{24}$$

In addition the kinematic condition boundary condition on the object gives

$$\tilde{Y} = \frac{\varepsilon}{2}(\tilde{X}^2 - 1), \text{ for } 0 < t < 1. \tag{25}$$

At the separations points $t = 0$ and $t = 1$ we must satisfy both (23) and (25), so we have

$$\frac{1}{2}\left(\frac{\tilde{\phi}_t}{s_b - s_a}\right)^2 + \frac{\varepsilon(\tilde{X}^2 - 1)}{2F^2} = \frac{1}{2}, \text{ for } t = 0 \text{ or } t = 1. \tag{26}$$

For the numerical computation we introduce again N equally-spaced points $t_1 = -e(N-1)/2$, $t_i = t_1 + e(i-1)$, $i = 2, ..., N$ and use the notation $x_i = \tilde{X}(t_i)$, $y_i = \tilde{Y}(t_i)$, $\phi_i = \tilde{\phi}(t_i)$,$x'_i = \tilde{X}'(t_i)$, $y'_i = \tilde{Y}'(t_i)$ and $\phi'_i = \tilde{\phi}_t(t_i)$.

The values of $\tilde{\phi}_t$ at the surface of the object cannot be determined as in (18), by using Bernoulli equation. At the surface of the object, between $t = 0$ and $t = 1$ there are $M = \frac{1}{e} - 1$ mesh points (we choose e such that $1/e$ is integer, but this is not a necessary condition). At each of them then are two unknowns ϕ'_i and y'_i. So we have $N + M + 2$ unknowns: $y'_1, ..., y'_N$, $\phi'_{\frac{N+1}{2}+1}, ..., \phi'_{\frac{N+1}{2}+M}$ and s_a, s_b.

The integral equation is evaluated at midpoints $t_{i-1/2}$, $i = 2, ..., N-1$ as before, so we obtain $N - 2$ equations. Another M equations are given by

$$y_{\frac{N+1}{2}+j} = \frac{\varepsilon}{2}(x^2_{\frac{N+1}{2}+j} - 1), \qquad j = 1, ..M. \tag{27}$$

The equations at the separation points (26) gives us another two equations and the radiation condition (19) gives us the last two equations. It should be noted that the values of $\tilde{\phi}'$ at the separation points ($\phi'_{\frac{N+1}{2}}$ and $\phi'_{\frac{N+1}{2}+M+1}$) are obtained using an extrapolation formula with 4 points (taken from the object).

The usual initial guess is $y'_i = 0$, $i = 1, ..., N$, $s_a = -1$, $s_b = 1$, $\phi'_{\frac{N+1}{2}+j} = s_b - s_a$, $j = 1, ..., M$.

At the first point we impose

$$y_1 = 0, x'_1 = \phi'_1 = s_b - s_a, x_1 = \phi_1 = s_a + (s_b - s_a)t_1, \tag{28}$$

and the remaining functions are calculated as before, using the equations (23)-(24) and the trapezoidal rule. The values of functions at midpoints are calculated again by interpolation with two points.

The numerical scheme described above was used to calculate solutions for various values of F and ε. The accuracy of the results was checked by varying N and e. We present typical free-surfaces for $\varepsilon > 0$ and for $\varepsilon < 0$ in Fig. 2. It can be observed that if we keep F constant and we vary the value of ε, the wavelength of the waves downstream does not change much, only the amplitude is affected.

Our calculations cannot be directly compared with those of Asavanant & Vanden-Broeck [11] because their study is for finite depth. Also they choose the position of the separation points and obtain the position of the vertex of the obstacle as part of the solution. In our case the position of the vertex of the object is known and we calculate the position of the separation points as part of the solution.

4 Three dimensional free surface flows

The results of the previous section shows that two dimensional free surface flows can be computed accurately by using the Green formulation. In this section we extend the ap-

proach for three dimensional flows. We present explicit results for pressure distributions and submerged objects.

4.1 Formulation

We consider a three dimensional distribution of pressure moving at a constant velocity U at the surface of a fluid of infinite depth. The sketch of the flow is given in Fig. 3. As in Section 2, we choose a frame of reference moving with the pressure distribution and assume that the flow is steady. We introduce cartesian coordinates x, y, z with the z-axis directed vertically upwards and the x-axis in the opposite direction of the velocity U. We denote by $z = \zeta(x, y)$ the equation of the free surface. The potential function $\Phi(x, y, z)$ satisfies Laplace equation

$$\nabla^2\Phi = 0, \qquad x, y \in \mathbf{R}, z < \zeta(x, y), \tag{29}$$

in the flow domain.

The kinematic boundary condition (3), the dynamic boundary condition (4) and the radiation condition (5) can now be rewritten as

$$\Phi_x\zeta_x + \Phi_y\zeta_y = \Phi_z, \quad z = \zeta(x, y), \tag{30}$$

$$\frac{1}{2}(\Phi_x^2 + \Phi_y^2 + \Phi_z^2) + g\zeta + \frac{p}{\rho} = \frac{U^2}{2}, \quad z = \zeta(x, y), \tag{31}$$

$$\text{no waves} \quad \text{as} \quad x \to -\infty. \tag{32}$$

Equation (10) holds in three dimensions where V represents a volume bounded with the surface C. Proceeding as in Section 2 and using the three dimensional free surface Green function

$$G = \frac{1}{4\pi}\frac{1}{((x - x^*)^2 + (y - y^*)^2 + (z - z^*)^2)^{1/2}} \tag{33}$$

we obtain

$$\frac{1}{2}(\phi(x^*, y^*) - Ux^*) = \int\int_{\mathbf{R}^2}(\phi(x, y) - Ux)\frac{1}{4\pi}\frac{\zeta(x, y) - \zeta(x^*, y^*) - (x - x^*)\zeta_x - (y - y^*)\zeta_y}{((x - x^*)^2 + (y - y^*)^2 + (\zeta(x, y) - \zeta(x^*, y^*))^2)^{3/2}}dxdy +$$

$$+ \int\int_{\mathbf{R}^2}\frac{1}{4\pi}\frac{U\zeta_x}{((x - x^*)^2 + (y - y^*)^2 + (\zeta(x, y) - \zeta(x^*, y^*))^2)^{1/2}}dxdy \tag{34}$$

where $\phi(x, y) = \Phi(x, y, \zeta(x, y))$.

We choose the pressure as

$$p(x, y) = \begin{cases} P_0 e^{\frac{L^2}{(x^2 - L^2)} + \frac{L^2}{(y^2 - L^2)}}, & |x| < L \text{ and } |y| < L \\ 0, & \text{otherwise} \end{cases}$$

We introduce dimensionless variables by using U as the unit velocity and L as the unit length. Combining equations (30) and (31) and using the chain rule of calculus we obtain

$$\frac{1}{2}\frac{(1 + \zeta_x^2)\phi_y^2 + (1 + \zeta_y^2)\phi_x^2 - 2\zeta_x\zeta_y\phi_x\phi_y}{1 + \zeta_x^2 + \zeta_y^2} + \frac{\zeta}{F^2} + \varepsilon P = \frac{1}{2} \tag{35}$$

where $F = U/(gL)^{1/2}$ and $\varepsilon = \frac{P_0}{\rho U^2}$. Now $P(x,y)$ is $e^{\frac{1}{x^2-1}+\frac{1}{y^2-1}}$ for $|x| < 1$ and $|y| < 1$, and 0 otherwise.

Equation (34) is now rewritten as

$$2\pi(\phi(x^*,y^*) - x^*) = I_1 + I_2 \tag{36}$$

where

$$I_1 = \int_0^\infty \int_{-\infty}^\infty (\phi(x,y) - \phi(x^*,y^*) - x + x^*)K_1 dxdy, \tag{37}$$

$$I_2 = \int_0^\infty \int_{-\infty}^\infty \zeta_x(x,y)K_2 dxdy \tag{38}$$

$$\begin{aligned} K_1 = &\left[\frac{\zeta(x,y) - \zeta(x^*,y^*) - (x-x^*)\zeta_x - (y-y^*)\zeta_y}{((x-x^*)^2 + (y-y^*)^2 + (\zeta(x,y) - \zeta(x^*,y^*))^2)^{3/2}} + \right. \\ &\left. + \frac{\zeta(x,y) - \zeta(x^*,y^*) - (x-x^*)\zeta_x - (y+y^*)\zeta_y}{((x-x^*)^2 + (y+y^*)^2 + (\zeta(x,y) - \zeta(x^*,y^*))^2)^{3/2}}\right] \\ K_2 = &\left[\frac{1}{\sqrt{(x-x^*)^2 + (y-y^*)^2 + (\zeta(x,y) - \zeta(x^*,y^*))^2}} + \right. \\ &\left. + \frac{1}{\sqrt{(x-x^*)^2 + (y+y^*)^2 + (\zeta(x,y) - \zeta(x^*,y^*))^2}}\right] \end{aligned} \tag{39}$$

In deriving (36) we used the fact that the solutions are symmetric in y direction. We note that the integral I_2 is singular whereas I_1 is not.

4.2 The numerical scheme

We truncate the intervals $-\infty < x < \infty$ and $0 < y < \infty$ to $x_1 < x < x_N$, and $y_1 < y < y_M$ and introduce the mesh points $x_i = x_1 + (i-1)dx$, $i = 1, \ldots, N$ and $y_j = (j-1)dy$, $j = 1, \ldots, M$. Following Forbes [1] the integral I_2 is written in the form $I_2 = I_2^{'} + I_2^{''}$:

$$I_2^{'} = \int_{y_1}^{y_M} \int_{x_1}^{x_N} (\zeta_x(x,y)K_2 - \zeta_x(x^*,y^*)S_2)dxdy$$

$$I_2^{''} = \zeta_x(x^*,y^*) \int_{y_1}^{y_M} \int_{x_1}^{x_N} S_2 dxdy$$

where

$$\begin{aligned} S_2 = &\frac{1}{\sqrt{A(x-x^*)^2 + B(x-x^*)(y-y^*) + C(y-y^*)^2}} \\ &+ \frac{1}{\sqrt{A(x-x^*)^2 - B(x-x^*)(y+y^*) + C(y+y^*)^2}} \end{aligned}$$

where

$$A = 1 + \zeta_x^2(x^*, y^*), B = 2\zeta_x(x^*, y^*)\zeta_y(x^*, y^*), C = 1 + \zeta_y^2(x^*, y^*).$$

The integral I_2'' (which contains the singularity) can be calculated using

$$\iint \frac{dsdt}{\sqrt{As^2 + Bst + Ct^2}} = \frac{t}{\sqrt{A}} \ln(2As + Bt + 2\sqrt{A(As^2 + Bst + Ct^2)}) +$$

$$+ \frac{s}{\sqrt{C}} \ln(2Ct + Bs + 2\sqrt{C(As^2 + Bst + Ct^2)}).$$

The $2NM$ unknowns are

$$\mathbf{u} = (\zeta_{x_{11}}, \zeta_{x_{12}}, \ldots, \zeta_{x_{N,M-1}}, \zeta_{x_{NM}}, \phi_{x_{11}}, \ldots, \phi_{x_{NM}})^T.$$

The integrals and the Bernoulli equation are evaluated at the points $(x_{i+1/2}, y_j)$, $i = 1, ..., N-1$, $j = 1, ..., M$ so we have $2(N-1)M$ equations. Another $2M$ equations are obtained from the radiation condition $\zeta_{x_{1j}} = 0, \phi_{x_{1j}} = 1$, $j = 1, \ldots, M$. The values of ζ and ϕ are obtained by integrating ζ_x and ϕ_x with respect to x by the trapezoidal rule. The integration is started by using the values derived from the radiation condition (32) and the free-surface condition (35) satisfied at the first row

$$\zeta_{1j} = 0, \zeta_{y_{1j}} = 0, \phi_{1j} = x_1, \phi_{y_{1j}} = 0, j = 1, .., M.$$

The values of ζ_y and ϕ_y are then calculated by central differences. The values of the variables ζ and ϕ at $(x_{i+1/2}, y_j)$ were obtained by interpolation

The $2nm$ nonlinear equations are solved by Newton's method. In most calculations we choose $\zeta_{x_{ij}} = 0, \phi_{x_{ij}} = 1$ for $i = 1, \ldots, N$, $j = 1, \ldots, M$ as the initial guess.

4.3 Results

We used the scheme of the Section 4.2 to calculate solutions for different values of the Froude number F and of the parameter ε. We found that the results are qualitatively similar. We present a typical free-surface profile for $F = 0.7$ and $\varepsilon = 1$ (see Fig. 4). The wake and the two different family of waves (transverse waves and short-length divergent waves) can be easily observed. When F increases the amplitude of the divergent waves becomes more important than that of the transverse waves (see Fig. 5). The wavelength of the transverse waves increases with the Froude number (see Fig. 6). Nonlinear solutions can be calculated close to the maximum height of waves allowed by Bernoulli equation.

The influence of the truncation upstream and downstream is seen to be negligible (see Fig. 7). Here we show the centerline (i.e. the intersection of the free surface with the plane $y = 0$). Two curves corresponding to different truncations $x = (-3, 12)$ and $x = (-6, 6)$ are shown.

The accuracy of the solutions have been tested by varying the number of grid points and the intervals dx and dy between grid points (see an example in Fig. 8). The upper part of the Figure, $y > 0$ is calculated with $N = 61$, $M = 17$, $dx = dy = 0.3$ and the

lower part $y < 0$ is calculated with $M = 89$, $M = 13$, $dx = dy = 0.2$. The values of the parameters are the same in both cases ($F = 0.7$, $\varepsilon = 1$).

The algorithm can be easily modified to include two or more pressure distributions and to study the interaction of the wakes produced by each of them. We present an example in Figure 9 for two pressure disturbances moving parallely. The V-shape of the waves downstream becomes in that case a W-shape. This case can be viewed as the wave interactions between ships moving parallely in deep water. A numerical study of wave interaction of two moving pressure disturbances in shallow water was done in Jiankang et al. [21], using a wave equation model.

There are various possible generalisations of our code. One of them is to calculate solutions in finite depth. In that case G should be replaced by

$$G = \frac{1}{4\pi} \frac{1}{((x-x^*)^2 + (y-y^*)^2 + (z-z^*)^2)^{1/2}} + \frac{1}{4\pi} \frac{1}{((x-x^*)^2 + (y-y^*)^2 + (z+z^*+2h)^2)^{1/2}}$$

where h is the depth of the fluid.

Another is to consider submerged objects. An inverse method to compute them is by superposing singularities. An example of the waves generated by a source and a sink is given in Fig. 10.

5 Conclusion

We have calculated two dimensional and three dimensional free surface flows generated by moving pressures. This models in an inverse way free surface flows past ships. For two dimensions we have presented a direct method using a parabolic object. The corresponding problem in three dimensions is left for future work. Generalisation for two pressure distributions and submerged disturbances were also presented.

Acknowledgements

This work was supported by EPSRC and the National Science Foundation.

References

[1] L. K. Forbes, An Algorithm for 3-Dimensional Free-Surface Problems in Hydrodynamics, Journal of Computational Physics 82 (1989) 330-347.

[2] D. C. Scullen and E. O. Tuck, Three-dimensional steady state nonlinear free-surface flow computation, Gazette of the Australian Mathematical Society 23 (1996) 80-84.

[3] E. O. Tuck, D. C. Scullen and L. Lazauskas , Ship-wave patterns in the spirit of Michell, IUTAM Symposium on Free-Surface Flows, Birmingham, July 2000. Proc. ed. A.C. King and Y.D. Shikhmurzaev, Fluid Mechanics and its Applications Volume 62, Kluwer Academic Publishers, Dordrecht, 2001, pp. 311–318.

[4] Y. Cao, W. W. Schultz, R. F. Beck, Three dimensional desingularized boundary integral methods for potential problems, Int. J. for Numer. Meth. Fluids 12 (1991) 785-803.

[5] S. Scorpio, R. Beck, F. Korsmeyer, Nonlinear water wave computations using a multipole accelerated, desingularized method, Proc. 21st Symp. Naval Hydro., Trondheim, Norway, June 1996, (National Academy Press, Washington D. C., 1997) 64-74.

[6] S. T. Grilli, P. Guyenne and F. Dias, A fully nonlinear model for three-dimensional overturning waves over arbitrary bottom. Int. J. for Numer. Meth. Fluids 35 (2001) 829-867.

[7] M. Xue, H. Xü, Y. Liu, D. K. P. Yue, Computations of fully nonlinear three-dimensional wave-wave and wave-body interactions. Part 1. Dynamics of steep three-dimensional waves, J. Fluid Mech. 438 (2001) 11-39.

[8] M. S. Longuet-Higgins, E. D. Cokelet, The deformation of steep surface waves on water: I. A numerical method of computation, Proc. R. Soc. Lond. A 350 (1976) 1-26.

[9] D. Nakos, P. Sclavounos, Ship motions by a three-dimensional Rankine panel method, Proc. 18th Symp. Naval Hydro., Ann Arbor, August 1990, (National Academy Press, Washington D. C., 1991) 21-40.

[10] W. T. Tsai, D. K. Yue, Computation of nonlinear free-surface flows, Ann. Rev. Fluid Mech. 28 (1996) 249-278.

[11] J. Asavanant, J.-M. Vanden-Broeck, Free-surface flows past a surface-piercing object, J. Fluid Mech. 273 (1994) 109-124.

[12] J.-M. Vanden-Broeck, F. Dias, Gravity-capillary solitary waves in water of infinite depth and related free-surface flows, J. Fluid Mech. 240 (1992) 549 - 557.

[13] L. K. Forbes, On the effects of non-linearity in free-surface flow about a submerged point vortex, J. Engng. Maths. 19 (1985) 139-155.

[14] J.-M. Vanden-Broeck, Steep solitary waves in water of finite depth with constant vorticity, J. Fluid Mech 274 (1994) 339-348.

[15] F. Dias, J.-M. Vanden-Broeck, Nonlinear bow flows with spray, J. Fluid Mech. 255 (1993) 91 - 102.

[16] G. C. Hocking, Bow flows with smooth separation in water of finite depth, J. Austral. Math. Soc. Ser. B 35 (1993) 114-126.

[17] D. E. Farrow, E. O. Tuck, Further studies of stern wavemaking, J. Austral. Math. Soc. Ser. B 36 (1995) 424-437.

[18] S. W. McCue, L. K. Forbes, Bow and stern flows with constant vorticity, J. Fluid Mech. 399 (1999) 277-300.

[19] M. A. D. Madurasinghe, E. O. Tuck, Ship bows with continuous ans splashless flow attachment, J. Austral. Math. Soc. Ser. B 27 (1986) 442-452.

[20] E. O. Tuck, J.-M. Vanden-Broeck, Splashless bow flows in twp dimensions?, Proc. 15th Symp. Naval Hydro., Hamburg, September 1984, (National Academy Press, Washington D. C., 1985) 293-302.

[21] W. Jiankang, T. S. Lee, C. Shu, Numerical study of wave interaction generated by two ships moving parallely in shallow water, Comput. Methods. Appl. Mech. Engrg. 190 (2001) 2099-2110.

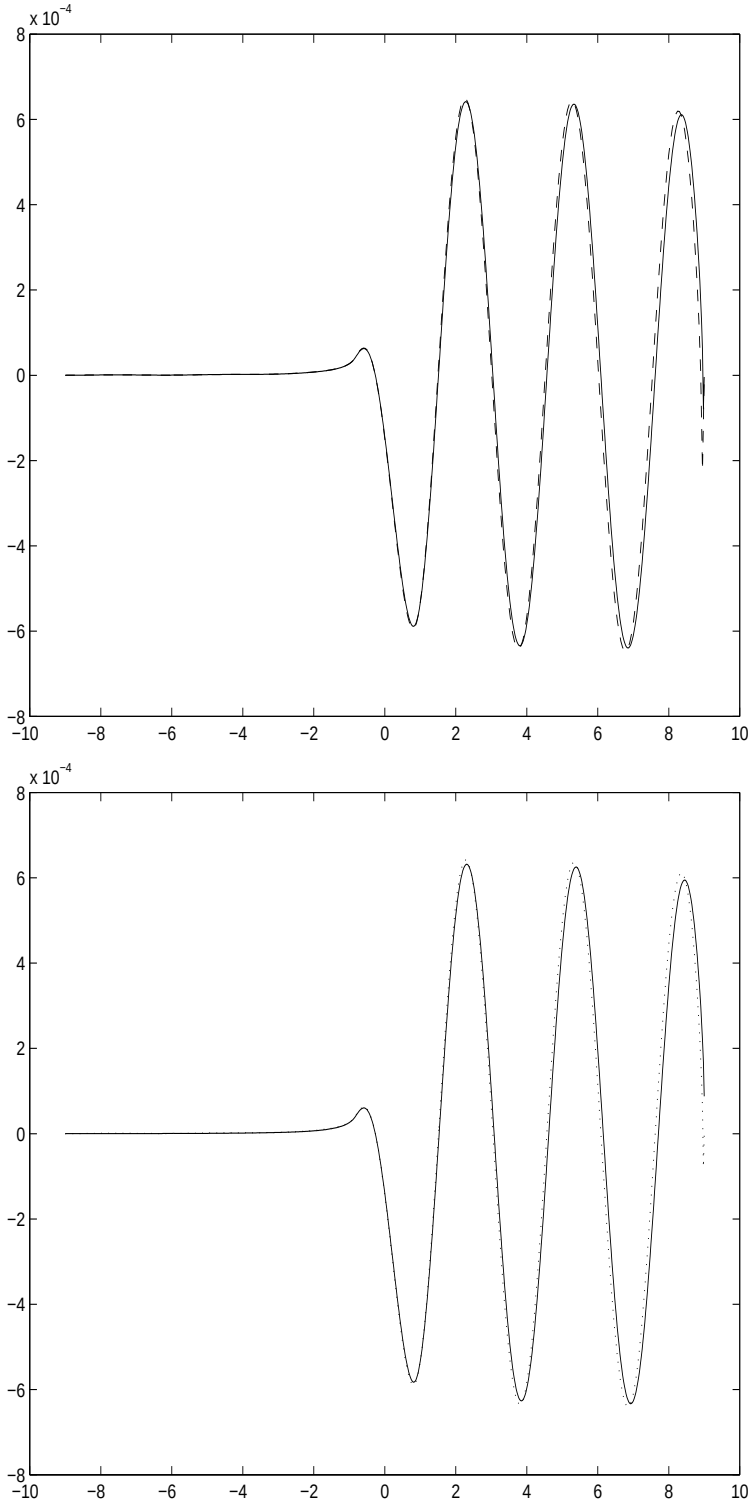

Figure 1: (top) Computed free-surface profiles obtained with the same parameters $F = 0.7, \varepsilon = 0.001$ but with different grids: N=721,e=0.025 (-) and N=361,e=0.05 (–) (bottom) Computed free-surface profiles obtained with this algorithm (-) and with an algorithm based on complex potential formulation (:). The parameters are $F = 0.7, \varepsilon = 0.001$ and the grid used: N=721, e=0.025.

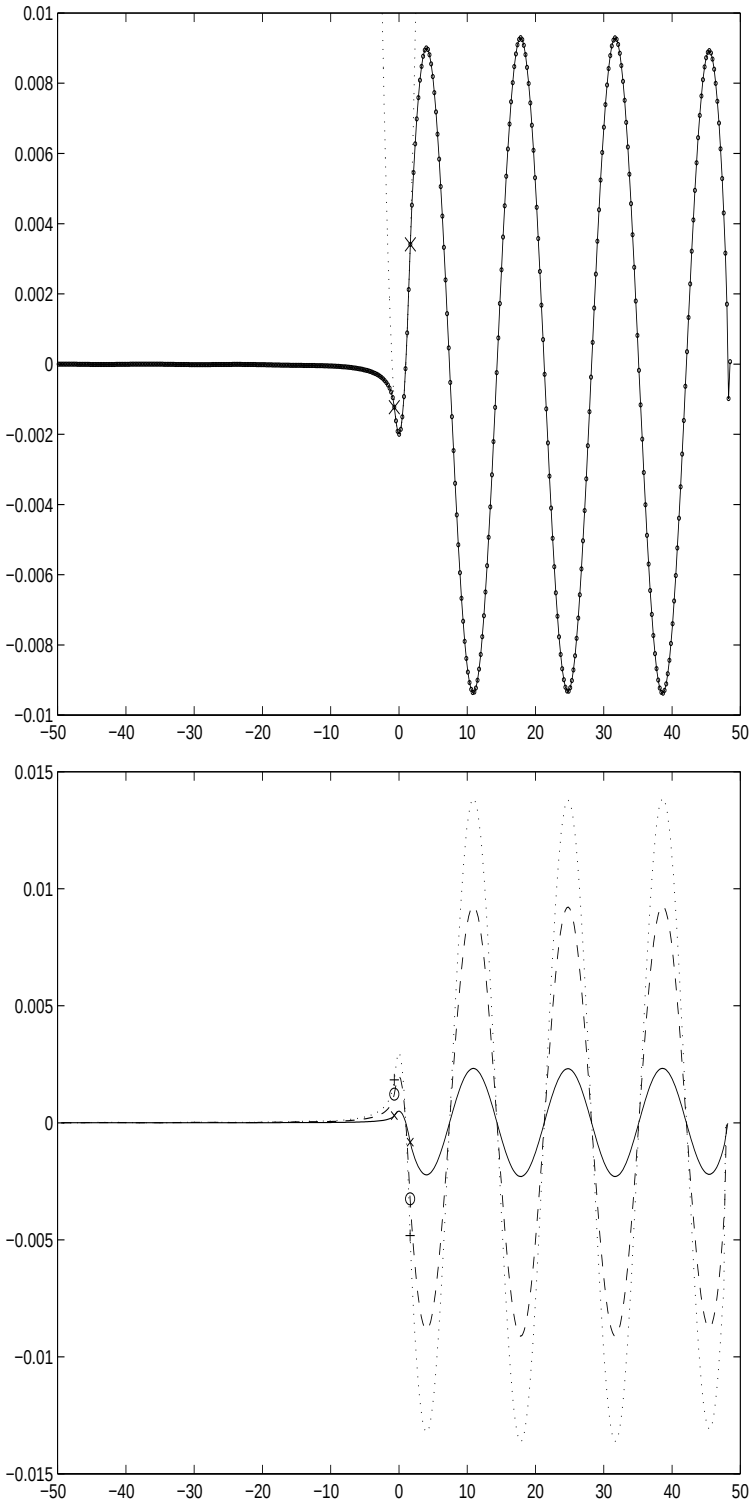

Figure 2: (top) Computed free-surface profiles obtained with $F = 1.5, \varepsilon = 0.004$ N=421,e=0.1. The parabolic object (:) and separation points ($\times$) are also showed. (bottom) Computed free-surface profiles obtained in the case $\varepsilon < 0$. The values of the parameters are $F = 1.5, \varepsilon = -0.006(:); \varepsilon = -0.004(--); \varepsilon = -0.001(-)$.

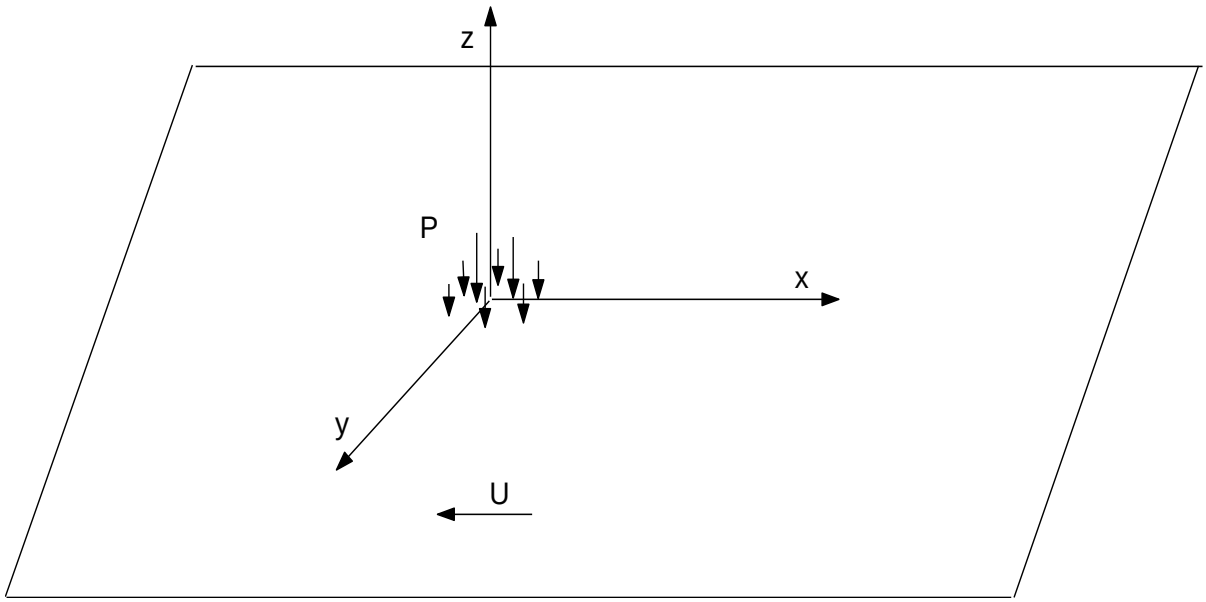

Figure 3: Sketch of the flow in the three dimensional case

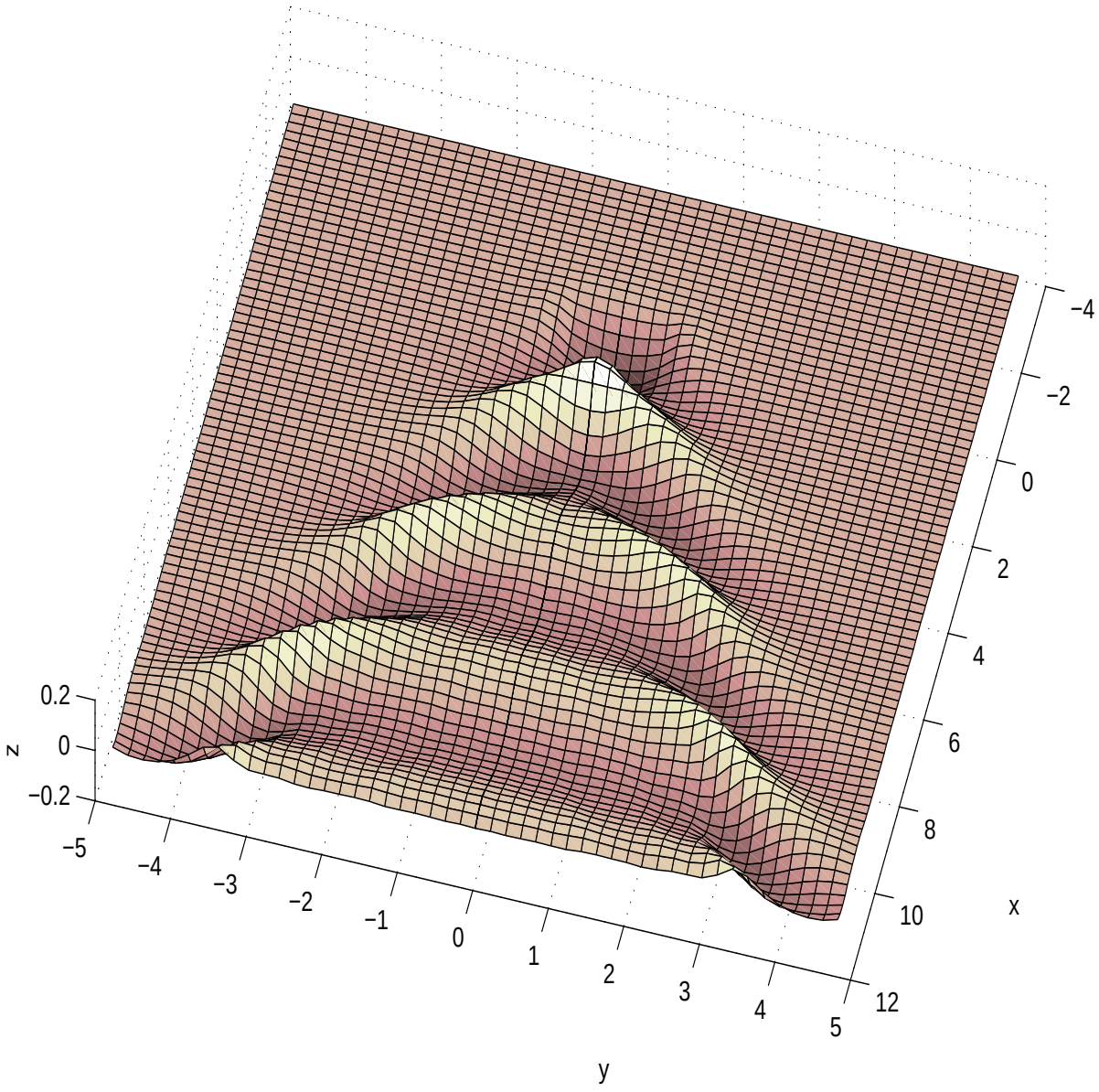

Figure 4: The solution for the wave field due to a moving pressure advancing at $F = 0.7$ and $\varepsilon = 1$. The grid used: N=75, M=25, dx=0.2, dy=0.2. The transverse waves are perpendicular to the direction of the velocity U (i.e. the x-axis). The divergent waves have crests roughly parallel to the direction of velocity, moving outward. In this graph and in the following three-dimensional figures the darker colors correspond to the troughs and the brighter colors to the peaks of the waves.

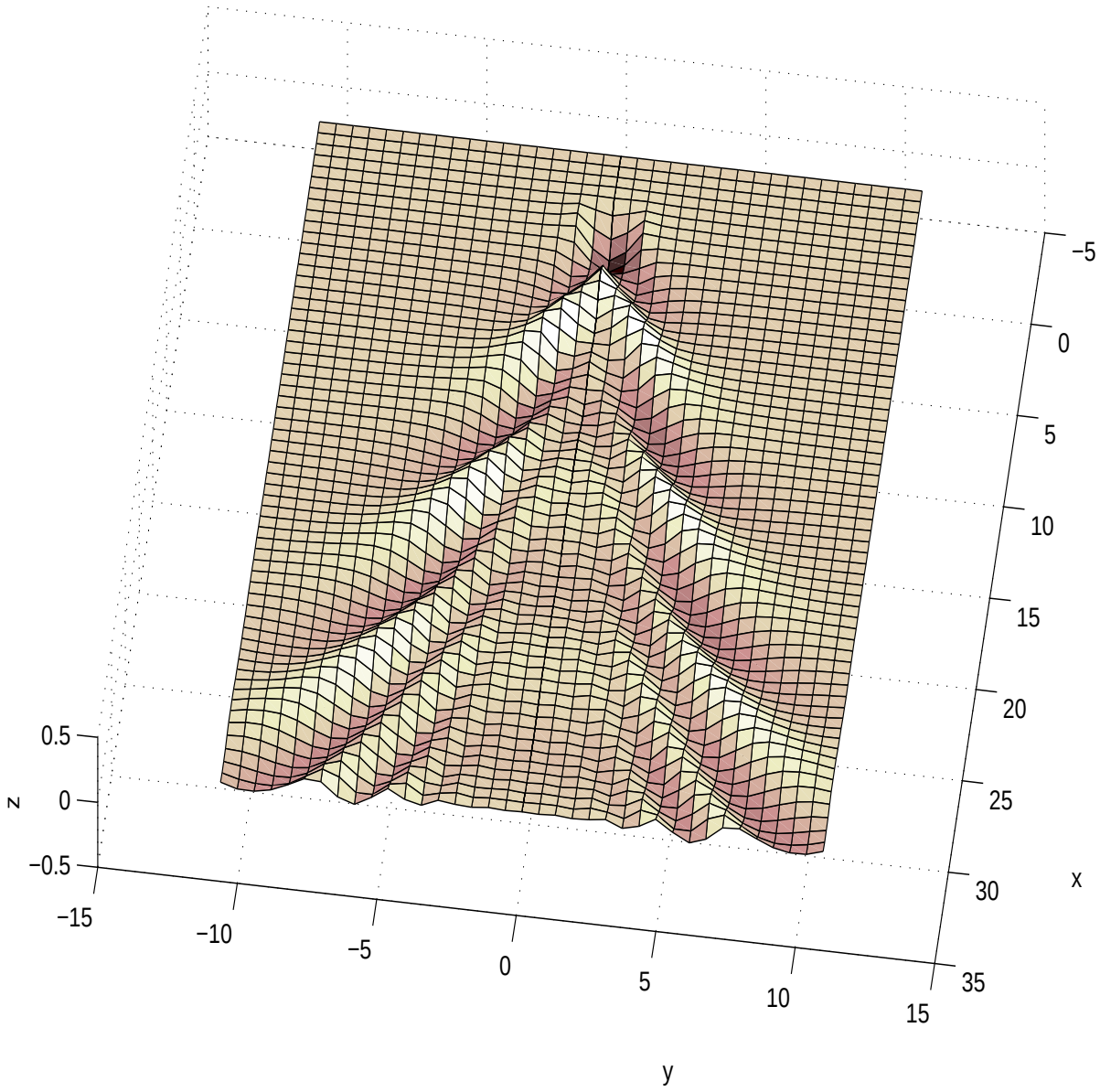

Figure 5: The waves generated for a higher Froude number ($F = 1.2$). The grid used: $N = 61$, $M = 19$, $dx = dy = 0.6$. The divergent waves can be observed more easily and their amplitudes are more important than those of the transverse waves.

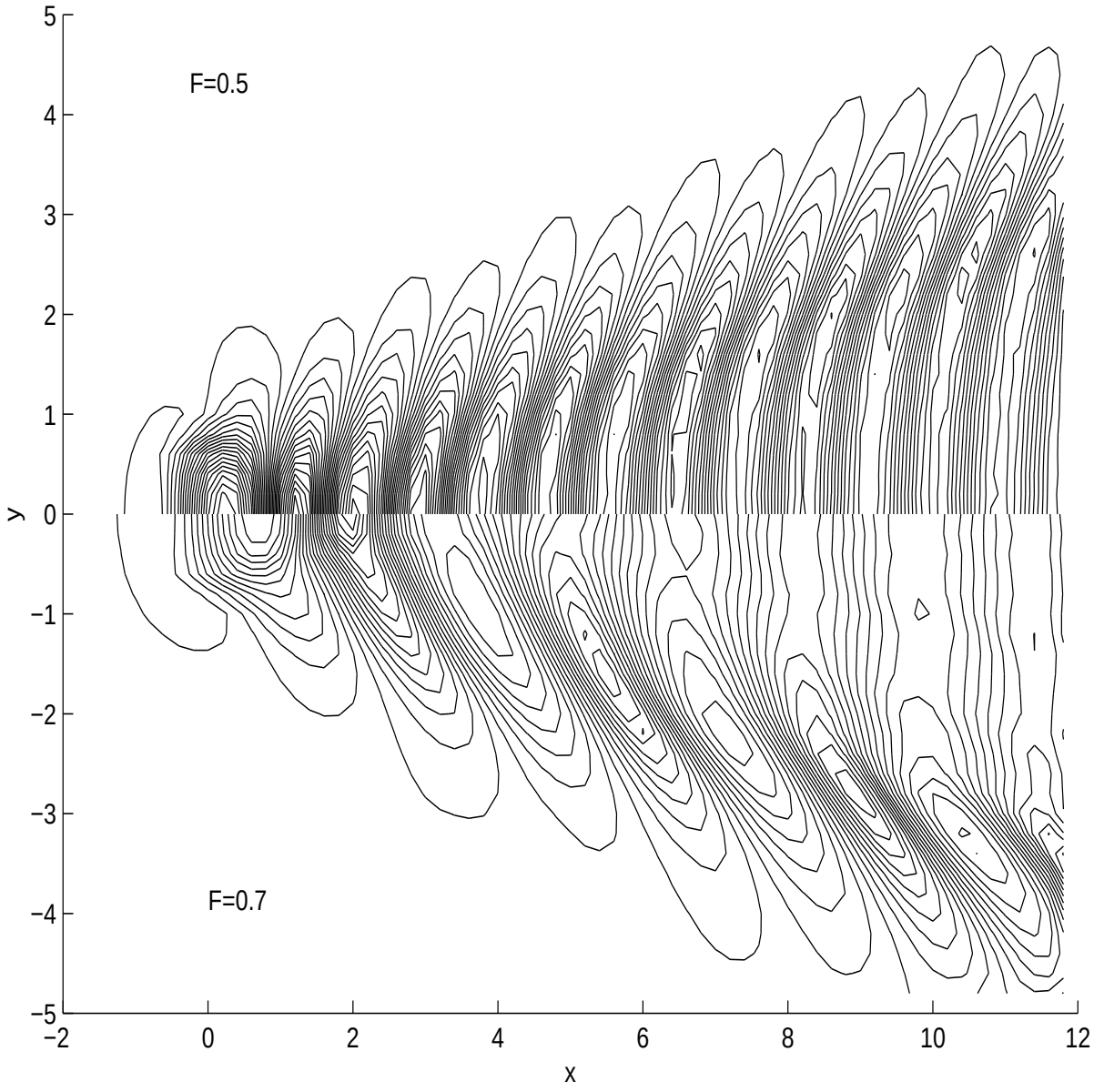

Figure 6: The wake in the cases $F = 0.7$ (lower half) and $F = 0.5$(upper half). In both cases $\varepsilon = 1$.

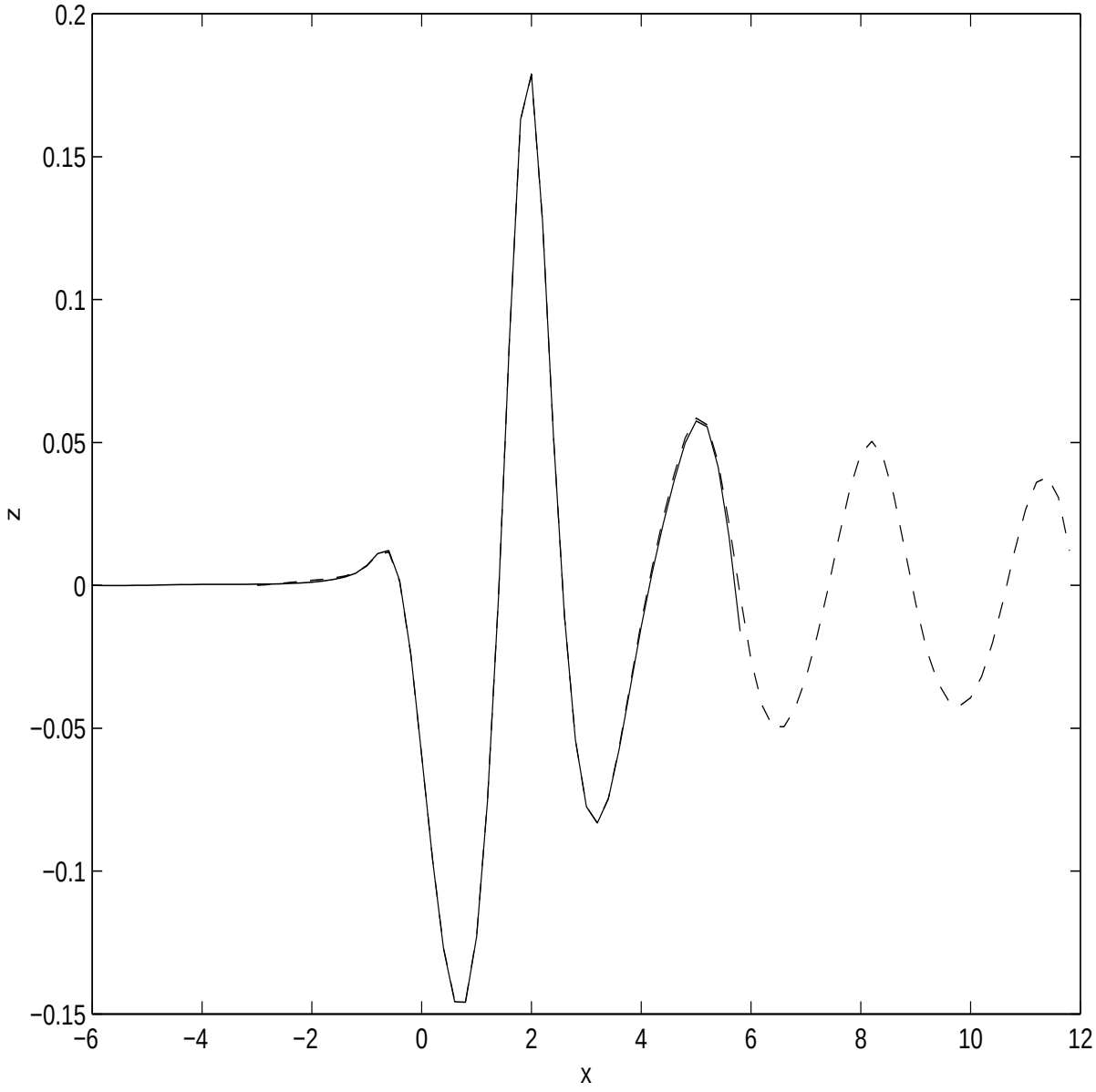

Figure 7: The free surface elevation at the plane $y = 0$ for two different truncations. Two curves corresponding to different truncations $x = (-3, 12)$ (the dashed line) and $x = (-6, 6)$ (the solid line) are shown. In both cases $F = 0.7, \varepsilon = 1$.

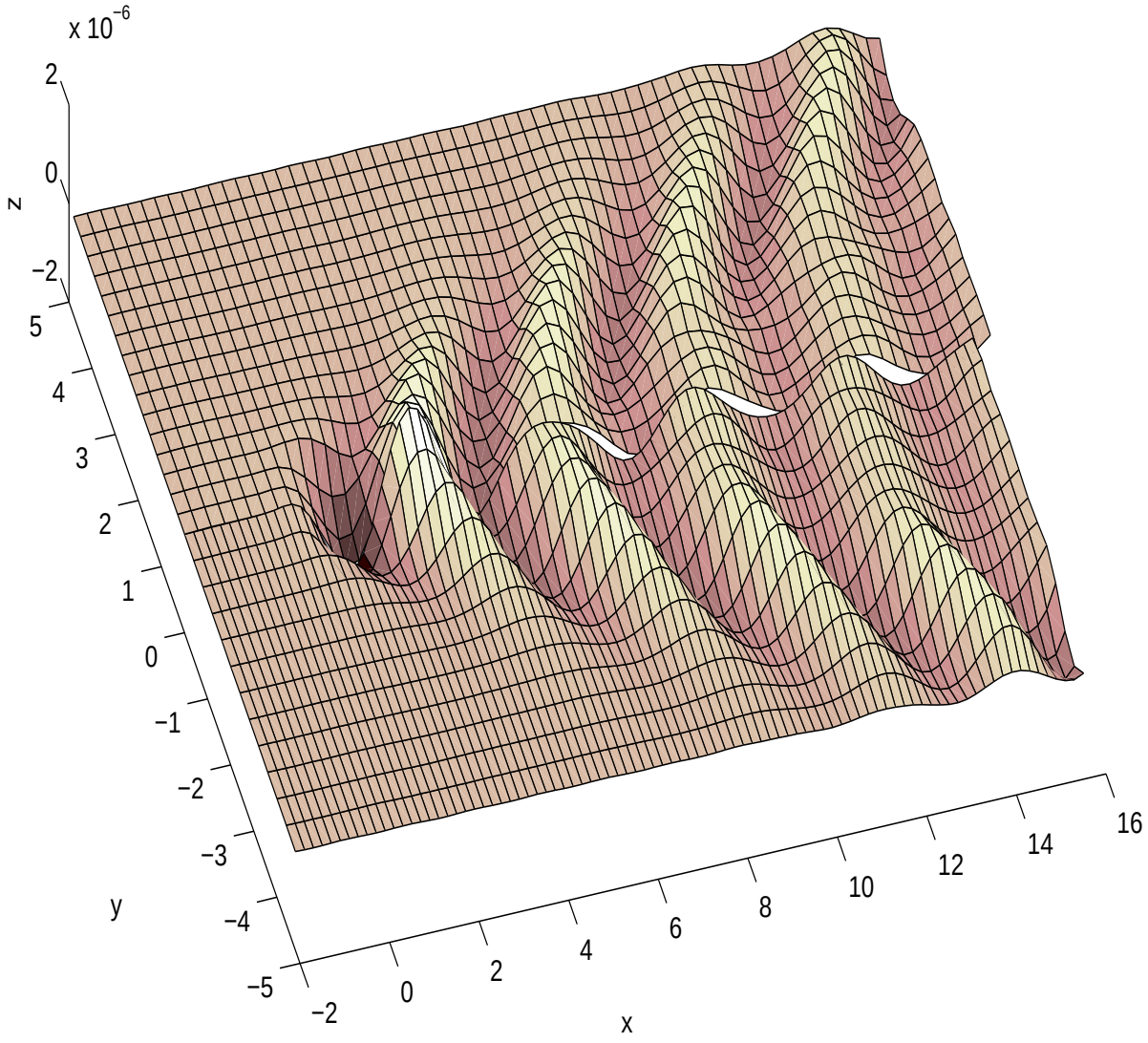

Figure 8: The accuracy check. $F = 0.7$, $\varepsilon = 1 \times 10^{-4}$, $N = 89$, $M = 13$, $dx = dy = 0.2$ (lower half), $N = 61$, $M = 17$, $dx = dy = 0.3$ (upper half).

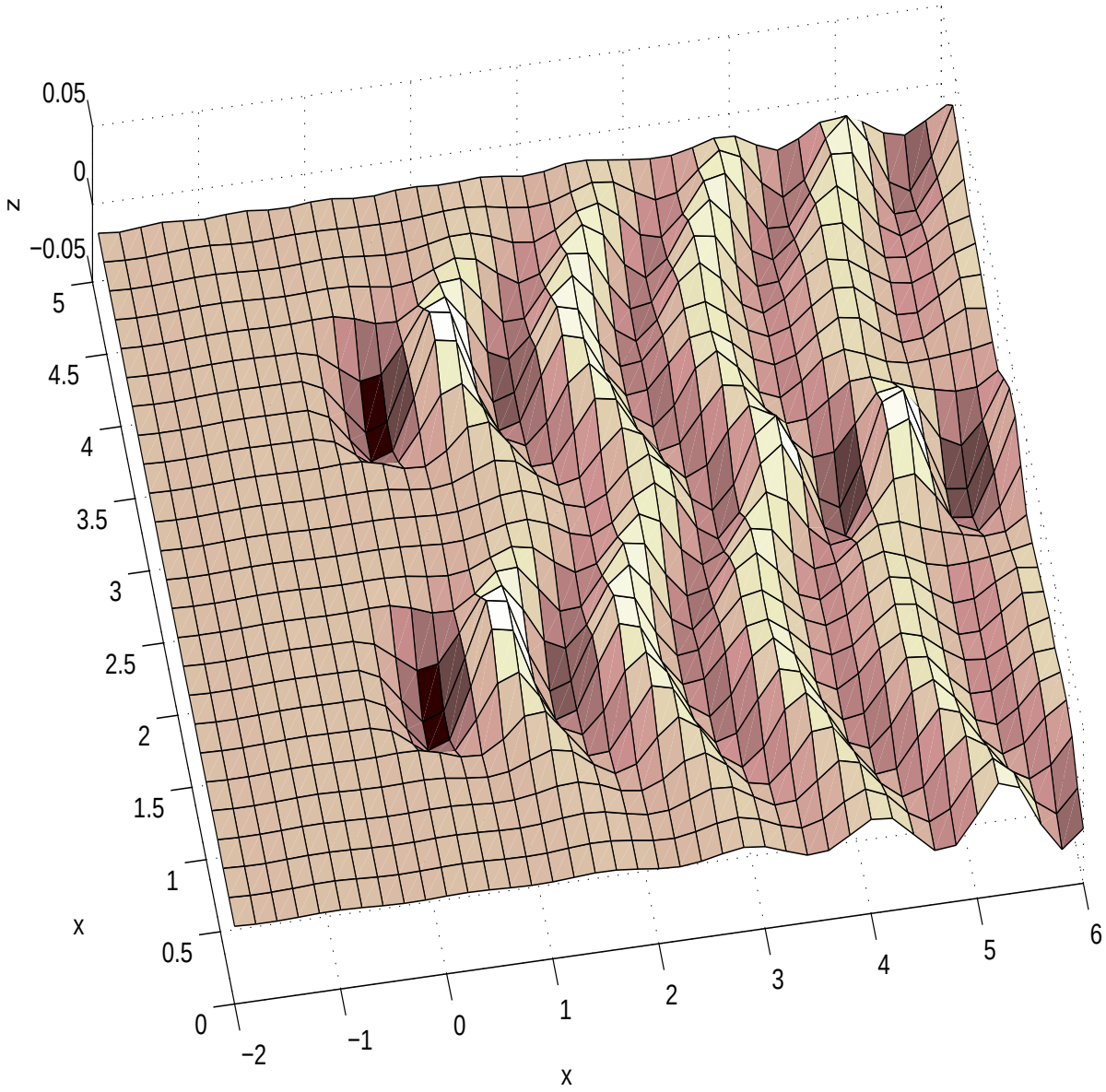

Figure 9: The case of two moving pressures ($F = 0.4$).

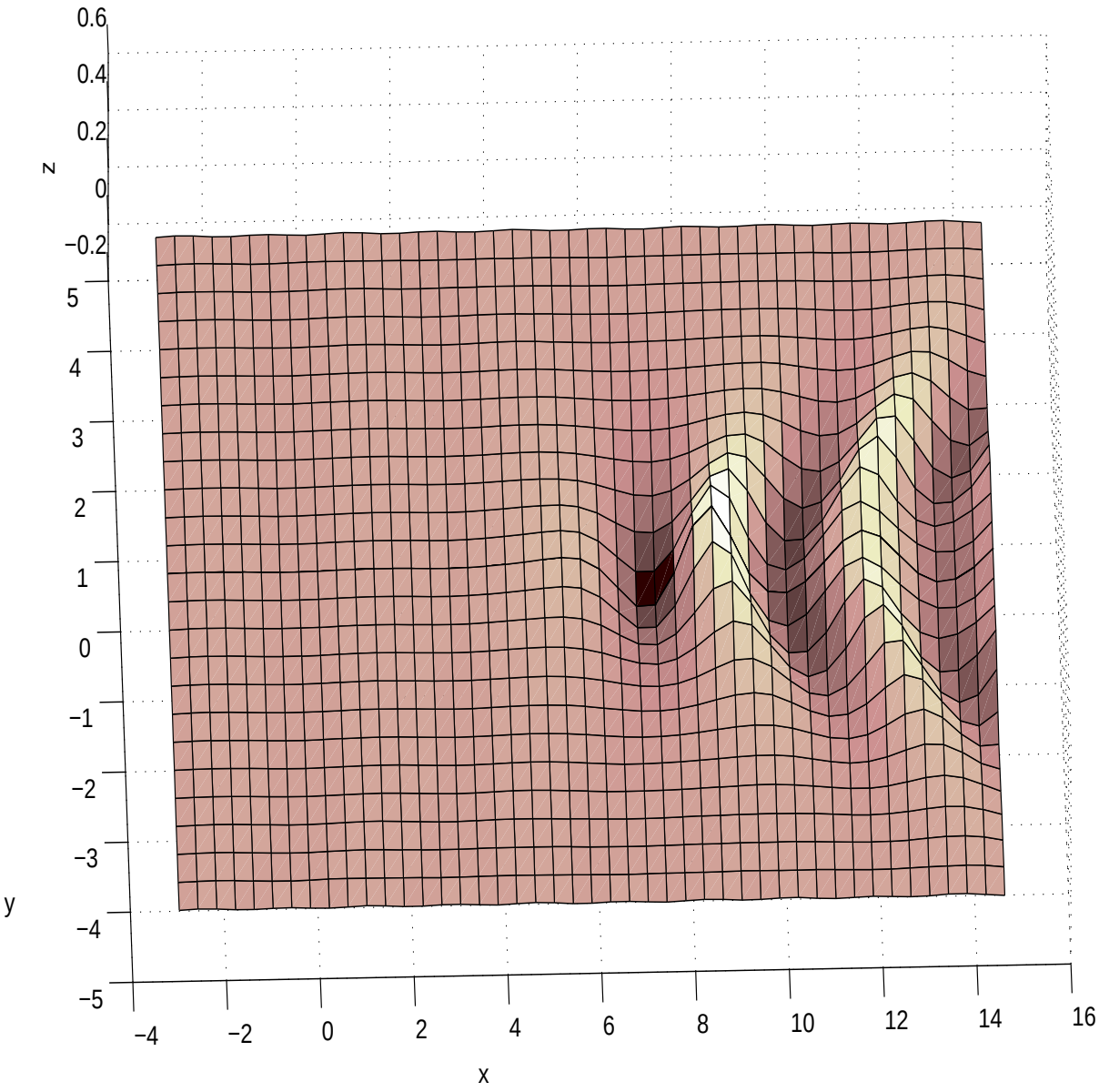

Figure 10: The waves generated by a pair source-sink ($F = 0.7$). The source is in (0,0,-1) and the sink in (1,0,-1)